# Supporting Information

# Silicon(lithiated)-sulfur full cells with porous silicon anode shielded by Nafion against polysulfides to achieve high capacity and energy density

Chenfei Shen[a,1], Mingyuan Ge[a,1,2], Anyi Zhang[a], Xin Fang[a], Yihang Liu[b], Jiepeng Rong[a], Chongwu Zhou[a,b,*]

[a]Mork Family Department of Chemical Engineering and Materials Science, University of Southern California, Los Angeles, California 90089, United States

[b]Ming Hsieh Department of Electrical Engineering, University of Southern California, Los Angeles, California 90089, United States

[*]Corresponding author.

Email address: chongwuz@usc.edu (C. Zhou).

[1]C. Shen and M. Ge contribute equally to this work.

[2]Present address: National Synchrotron Light Source II, Brookhaven National Laboratory, Upton, New York 11973, United States.

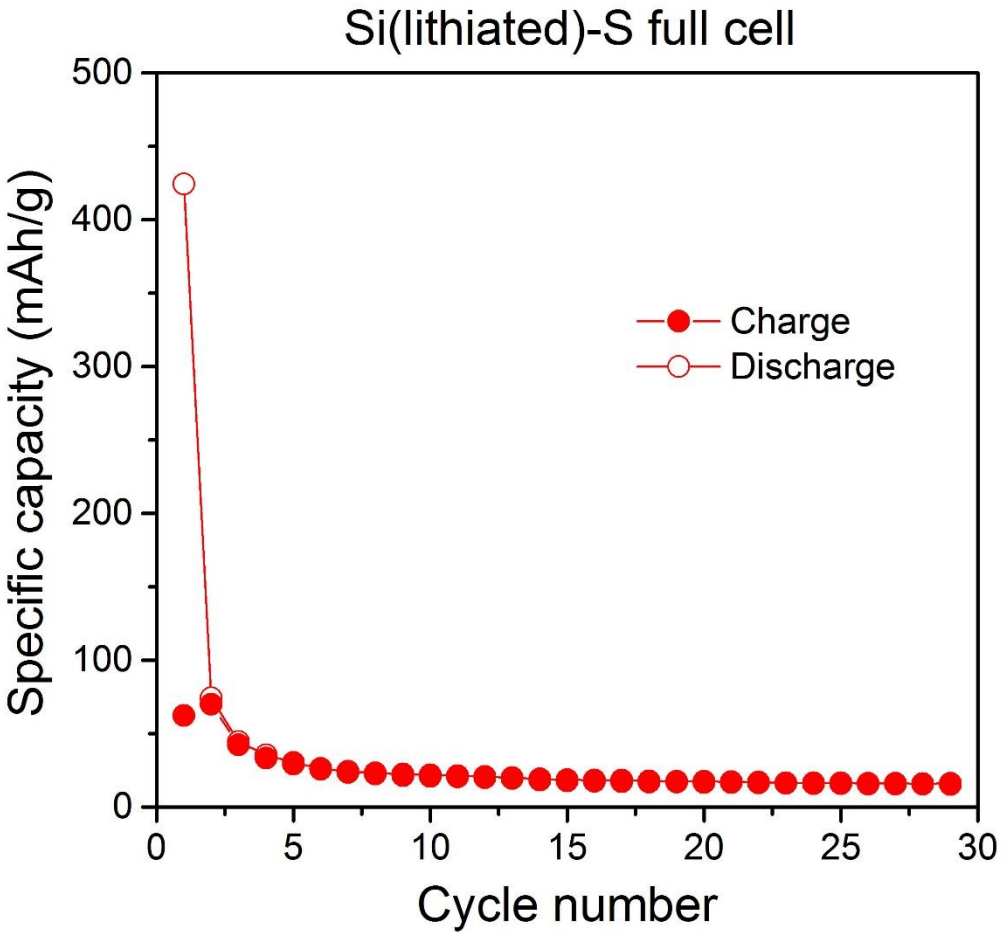


**Figure S1** Cyclic performance of Si-S full cell using lithiated bare porous Si as anode and S-C-G as cathode in the voltage window of 1.2-2.7 V (vs. $Li/Li^+$) at current density of 0.1 C. The electrolyte is LITFSI electrolyte (1 M LITFSI in DME/DOL, 1:1 by volume, with addition of 5% $LiNO_3$). The specific capacity of the Si-S full cell is calculated based on the mass of sulfur.

**EDS and XPS analyses of the reaction product of Si wafers and polysulfides electrolyte**

We have carried out EDS and XPS measurements to analyze the reaction product of Si wafers and polysulfides electrolyte. In the experiment, one piece of bare Si wafer was immersed in polysulfides electrolyte

for 12 h. The wafer was then washed with DME/DOL and dried in Ar-protected environment before characterization. Figure S2a shows the EDS spectrum of the Si wafer after reaction with polysulfides electrolyte, in which Si, S, and O signals are clearly resolved. Compared with the EDS spectrum of a bare Si wafer (Figure S2b), where only a peak corresponding to Si is observed, the presence of S signal in Figure S2a confirms the reaction between the Si wafer and polysulfides electrolyte, which results in the formation of complex Si-S compound. For comparison, we prepared a "polysulfides electrolyte sample" by dropping polysulfides electrolyte onto a Cu foil and dried it in vacuum oven so that the solutes in the electrolyte would be left on the Cu foil for EDS measurement. Compared with the EDS spectrum of pure polysulfides electrolyte (Figure S2c), the absence of F, N, and C signals in Figure S2a confirms that the polysulfides electrolyte is completely washed away from the Si wafer so that the S signal in Figure S2a is from the reaction product of Si wafer and polysulfides electrolyte. The O content in the electrolyte based on EDS spectrum (Figure S2c) is 28.3%, which is higher than 14.9% calculated based on chemical formulas of the solutes in the electrolyte. The excess O is believed to result from the oxidation of polysulfides during sample transferring process from the Ar-protected environment to the scanning electron microscope. Similarly, the O signal in Figure S2a is also due to oxidation of reaction product of Si wafer and polysulfides electrolyte during the sample transferring process.

Figure S2d-f show the Li 2s, S 2p, and Si 2p XPS spectra of a Si wafer after reaction with polysulfides electrolyte. For comparison, the Li 2s and S 2p XPS spectra of polysulfides electrolyte are shown in Figure S2g and S2h, and Si 2p XPS spectrum of a bare Si wafer is shown in Figure S2i. Firstly, we compare Figure S2d and S2g. The Li 1s peak at 55.9 eV in Figure S2g is assigned to $Li_xSO_y$, which demonstrates the oxidation of polysulfides electrolyte during the sample transferring process [1]. This is consistent with the EDS result in

Figure S2c, which demonstrates high O content in the electrolyte. In comparison, the $Li_xSO_y$ peak (blue curve) also shows up in the Li 1s spectrum of Si wafer after reaction with polysulfides electrolyte (Figure S2d). Since the electrolyte is completely washed away from the wafer before characterization, it is believed that the $Li_xSO_y$ in Figure S2d is from the reaction product between the Si wafer and polysulfides, which is consistent with the EDS result in Figure S2a. In addition, the peak at 52.9 eV in Figure S2d is assigned to $Li_xSi$, indicating that the reaction product also contains Li-Si bond [2]. From this comparison, we conclude that the reaction product contains both Li-Si and Li-S bonds. Further confirmation comes from the comparison of S 2p spectra for reaction product (Figure S2e) and polysulfides electrolyte (Figure S2h). In Figure S2h, the S 2p peak (composed of $2p_{3/2}$ and $2p_{1/2}$ due to spin-orbit coupling) at 169.6 eV (green curves) corresponds to LITFSI, and the peaks in the range of 166-160 eV are assigned to $Li_2S_x$ species in the polysulfides electrolyte [3]. The peak at 167.9 eV (magenta curves) may result from the formation of $Li_2SO_3$ or $Li_2SO_4$, and therefore we assign it to $Li_xSO_y$ [1,4,5]. This $Li_xSO_y$ peak indicates the oxidation of polysulfides during the sample transferring process, which is consistent with the EDS result in Figure S2c and XPS result in Figure S2g. By comparing Figure S2e and S2h, it is observed that the peaks which correspond to LITFSI and $Li_2S_x$ disappear in Figure S2e, confirming that the polysulfides electrolyte is completely washed away after reaction. On the contrary, a broad peak in the range of 172-162 eV is observed and can be deconvoluted to four sub-peaks. As shown in Figure S2e, the peak at 168.1 eV (red curves) may belong to $-SO_3$ or $-SO_4$ [1,4,5], and the peak at 165.6 eV (blue curves) may belong to $-S_2O_6$ [4]. It should be noted that due to the complex oxidation states of the S element, and possible effect of Si element on the bonding environment in the reaction product, the 172-162 eV broad peak may contain other sub-peaks with low intensity (not shown in the figure), which results in the relatively large peak splitting of $2p_{3/2}/2p_{1/2}$ doublets in Figure S2e, compared to the $Li_xSO_y$ $2p_{3/2}/2p_{1/2}$ doublet in Figure

S2h. For these reasons, we assign the 4 sub-peaks in Figure S2e as -$SO_x$. Finally, we have compared Figure S2f and S2i. As shown in Figure S2i, the Si 2p peak is composed of $2p_{3/2}$ (99.4 eV) and $2p_{1/2}$ (100.0 eV) spin-orbit components [6]. In contrast, the main peaks in Figure S2f located at 98.8 eV and 99.4 eV are assigned to $Li_xSi$ $2p_{3/2}$ and $2p_{1/2}$ components, respectively [7,8]. In addition, a broad peak centered at 101.5 eV is observed, which is assigned to $Li_xSiO_y$ [7,8].The existence of the $Li_xSi$ and $Li_xSiO_y$ peaks in Figure S2f provides further evidence that the reaction product contains Si element, which is consistent with the XPS result in Figure S2d. In summary, based on the EDS and XPS analyses, we conclude that the reaction product of Si wafers and polysulfides electrolyte is composed of Li, Si, and S.

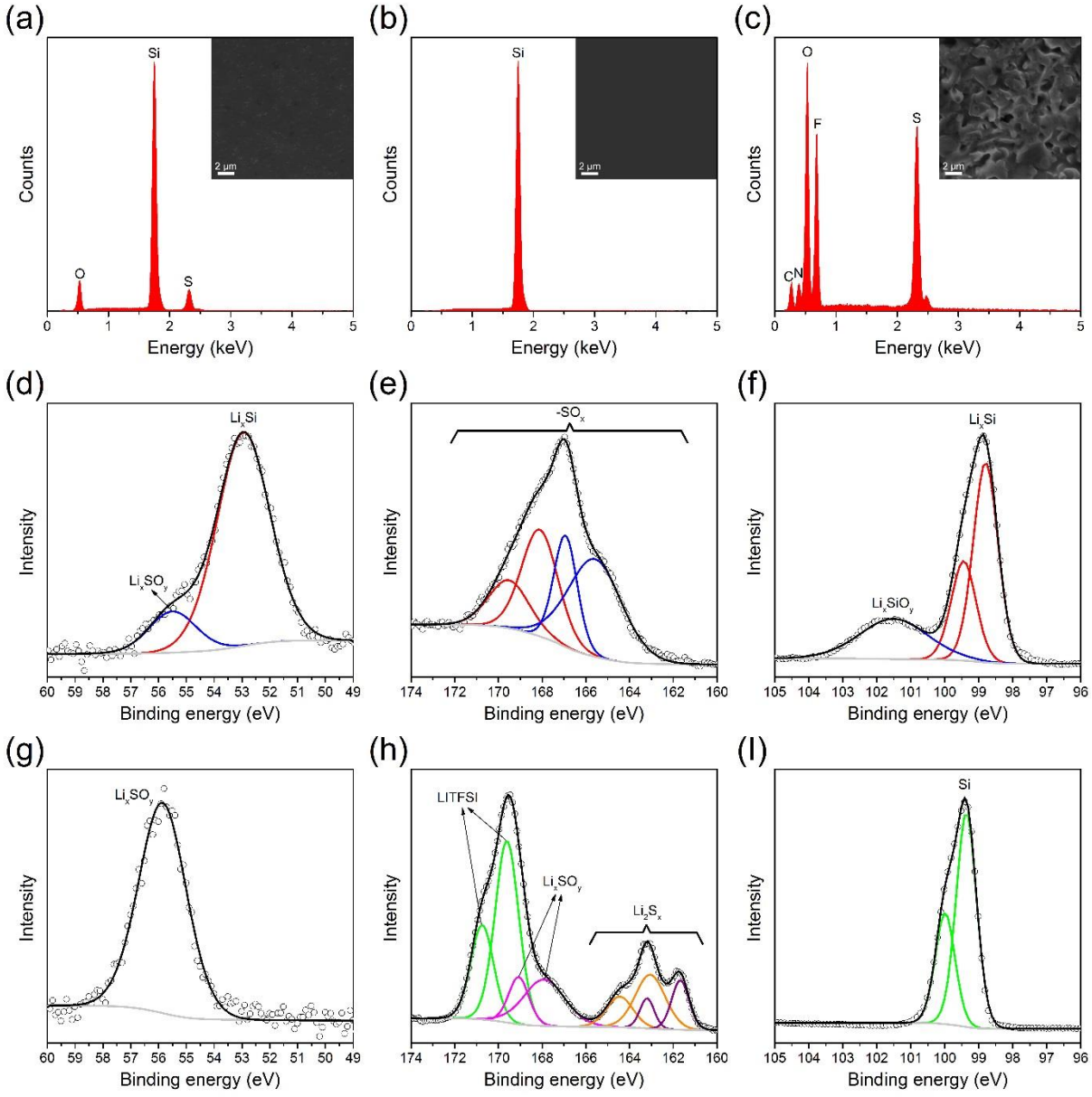


**Figure S2** EDS and XPS analyses of the reaction product of Si wafers and polysulfides electrolyte. (a-c) EDS spectra of a Si wafer after reaction with polysulfides electrolyte (a), a bare Si wafer (b), and polysulfides electrolyte (c). Insets show the SEM images of corresponding regions for collecting the EDS spectra. (d-f) Li 2s (d), S 2p (e), and Si 2p (f) XPS spectra of a Si wafer after reaction with polysulfides electrolyte. (g,h) Li 2s (g) and S 2p (h) XPS spectra of polysulfides electrolyte. (i) Si 2p XPS spectrum of a bare Si wafer. Hollow

circles: experimental data; gray lines: background; black lines: overall fit; colored lines: fitted individual components.

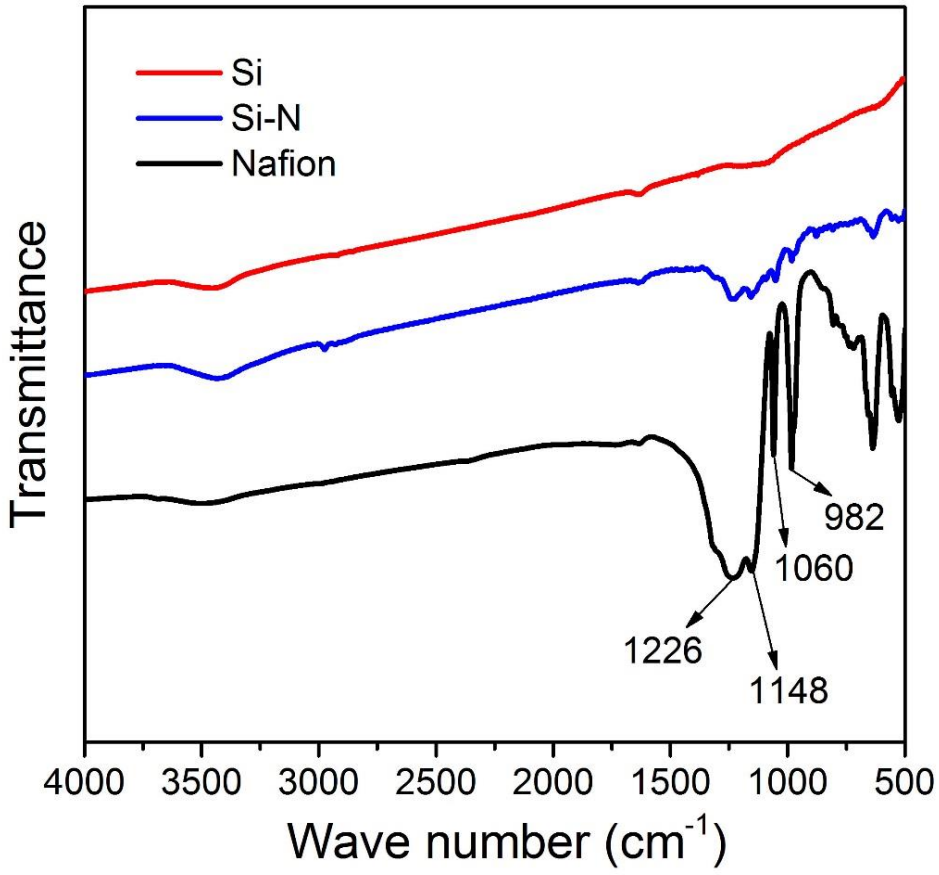


**Figure S3** FTIR spectra of Si, Si-N, and Nafion.

**Morphology and electrochemical performance of S-C-G**

Figure S4a and S4b show the SEM and TEM images of S-C-G. From Figure S4a and S4b, carbon nanofiber and graphene are clearly identified. The small particles are carbon black, and the bright region in SEM (Figure

S4a) and the dark region in TEM (Figure S4b) indicate the presence of sulfur. Figure S4c shows the cyclic performance of Li-S half cell in the voltage window of 1.7-2.7 V (vs. $Li/Li^+$) at current density of 0.1 C using S-C-G as working electrode. Figure S4d shows the charge-discharge curves of Li-S half cell using S-C-G as working electrode. The electrolyte is LITFSI electrolyte.

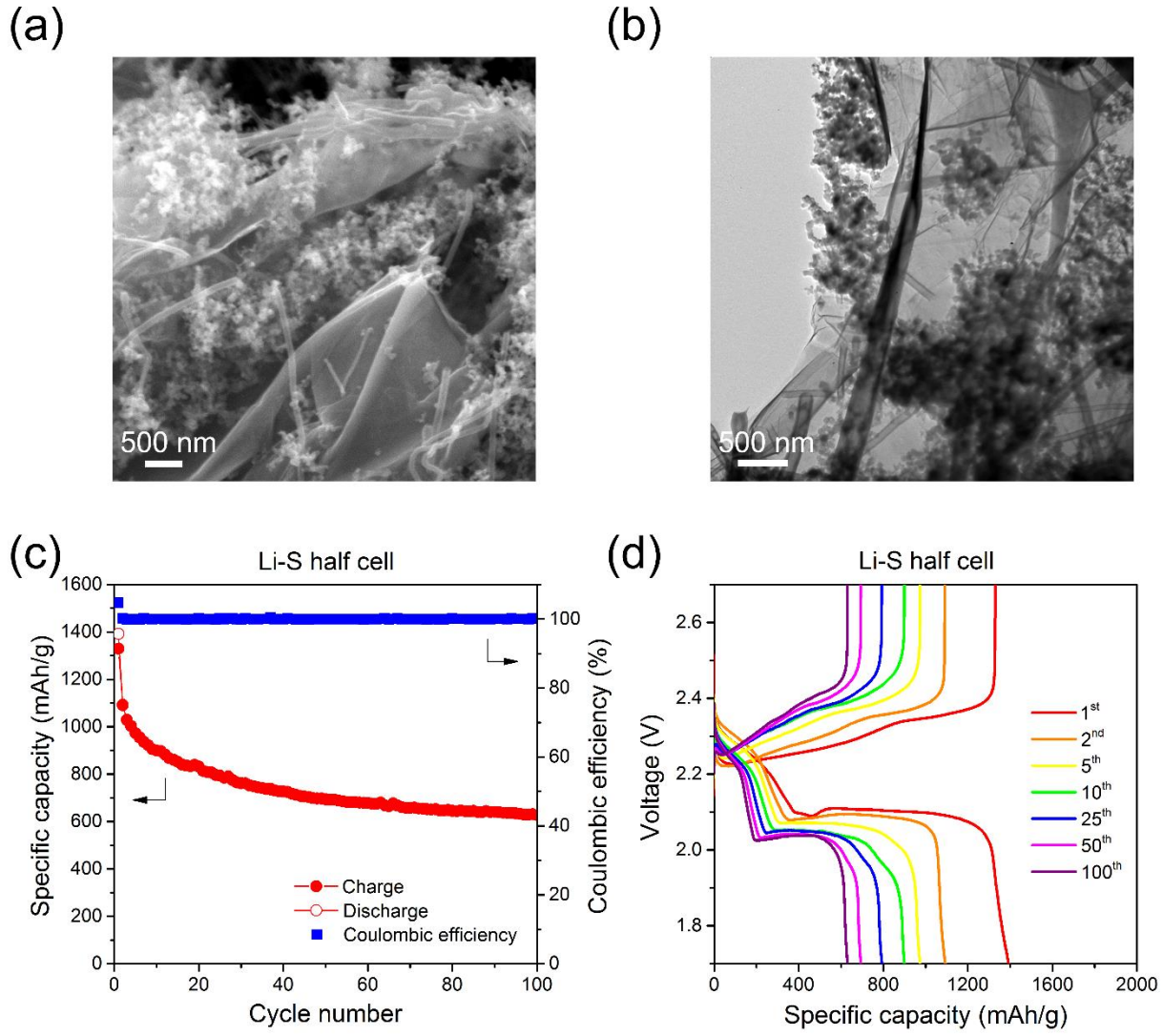


**Figure S4** (a) SEM and (b) TEM images of S-C-G. (c) Cyclic performance and (d) Charge-discharge curves of S-C-G.

**Morphology and electrochemical performance of Si-C-N-G**

Figure S5a and S5b show the SEM and TEM images of Si-C-N-G. From the images, it is clear to observe that the Si particles are well wrapped with graphene layers. Figure S5c shows the cyclic performance of Li-Si half cell in the voltage window of 0.01-2 V (vs. $Li/Li^+$) at current density of 400 mA/g using Si-C-N-G as working electrode. Figure S5d shows the charge-discharge curves of Li-Si half cell using Si-C-N-G as working electrode. The electrolyte is LITFSI electrolyte.

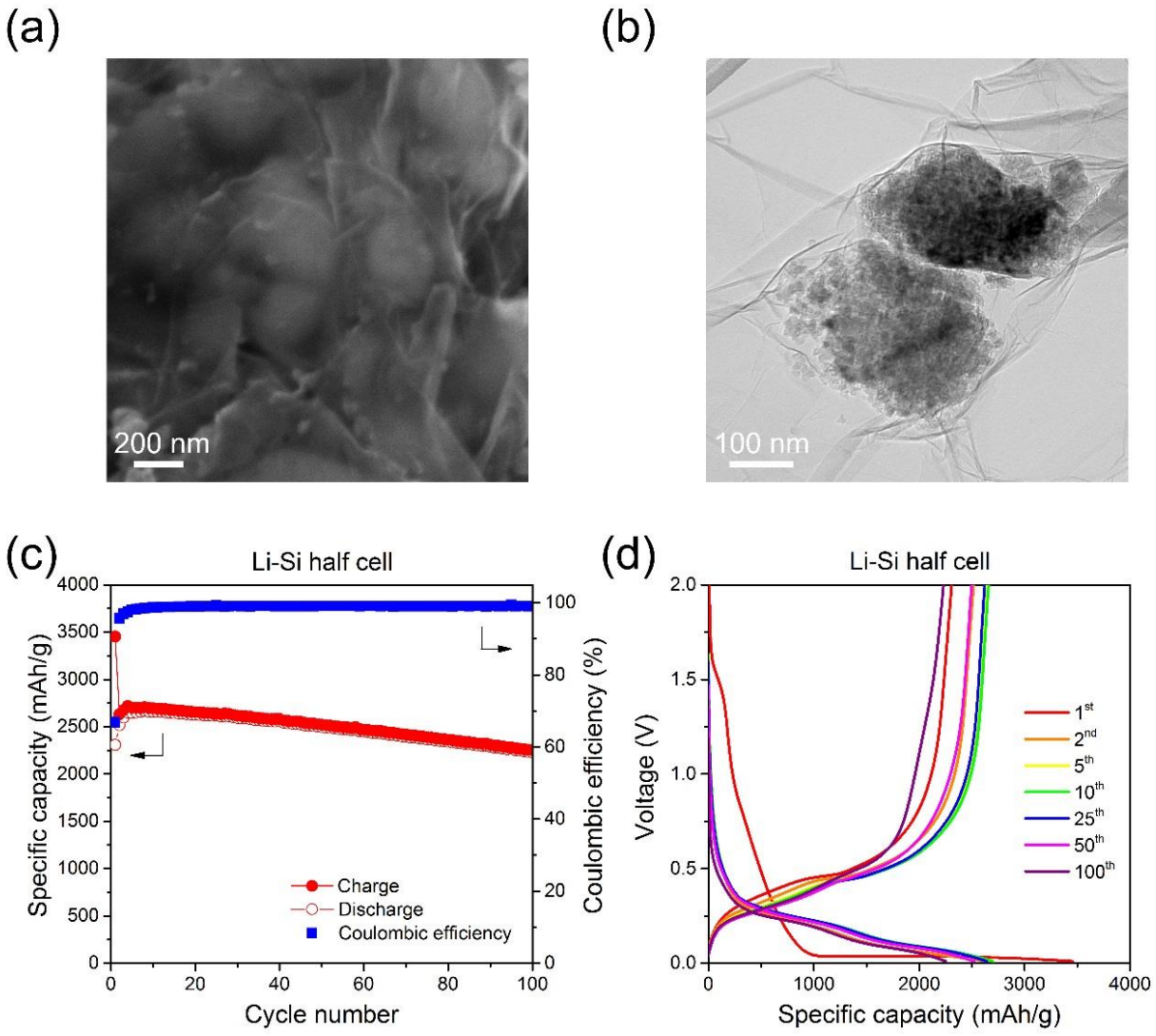


**Figure S5** (a) SEM and (b) TEM images of Si-C-N-G. (c) Cyclic performance and (d) Charge-discharge

curves of Si-C-N-G.

**Impedance tests of Si-C-G and Si-C-N-G**

To further elucidate the functionality of Nafion, we have conducted impedance measurements on both Si-C-G and Si-C-N-G in Li-Si half-cell configuration. The EIS were collected with an AC voltage of 5 mV amplitude in the frequency range of 1000 kHz to 10 mHz. Figure S6a shows the Nyquist plots of the cells after being rested for 24 hours. Conventionally, a typical Nyquist plot is composed of two semicircles at high frequency region and one linear diffusion drift at low frequency region. The high frequency semicircles are related to interfacial impedance due to the formation of SEI [9] and interphase electronic contact resistance (charge transfer resistance $R_{ct}$) [10]. However, in Figure S6a, only the semicircle corresponding to $R_{ct}$ is observed in the high frequency region (>1 kHz) for both Si-C-G and Si-C-N-G before cycling, which is attributed to the negligible formation of SEI layer [11]. The value of $R_{ct}$ can be read from the intercept of the semicircle with the Z-real axis. From Figure S6a, it is observed that the Nafion-coated sample (Si-C-N-G) has slightly larger $R_{ct}$ than that of the sample without Nafion coating (Si-C-G). It is mainly due to the additional resistance from Nafion coating. However, as the Nafion coating is rather thin (Figure 2d), the resistance increase is not significant. Figure S6b shows the Nyquist plots of both electrodes after 5 charge-discharge cycles (electrodes are at delithiated state for EIS measurements). For Si-C-G electrode, a new semicircle appears in the high-frequency region of the Nyquist plot, indicating the formation of thick SEI layer. Moreover, the radius of the semicircle corresponding to $R_{ct}$ becomes larger compared with that before cycling, suggesting larger charge transfer resistance of the electrode due to poor electric contact between Si-C-G particles [12]. It is supposed to result from the increased electric resistance of a thick and insulating SEI layer formed on

Si-C-G particle surface. On the contrary, the Si-C-N-G electrode still shows one semicircle and its radius is smaller compared with its pristine states before cycling, indicating reduced $R_{ct}$ of the electrode after cycling. This is because the Nafion coating on Si in Si-C-N-G electrode can prevent direct formation of SEI on Si surface. In addition, the loose structure of Nafion polymer provides 3-dimentional interconnected channels, which can significantly facilitate $Li^+$ ion diffusion from electrolyte to Si. In conclusion, Nafion coating not only helps to prevent Si (and lithiated Si) from reacting with polysulfides, but also reduces the electrode-electrolyte interface resistance, which contributes to good electrochemical performance of the Si-S full cell.

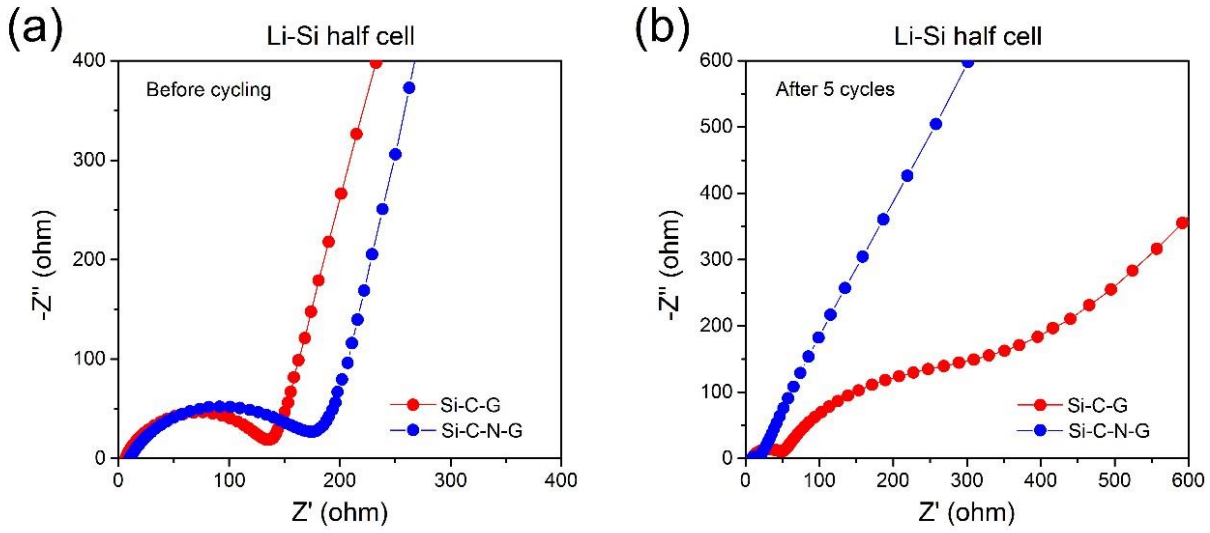


**Figure S6** Nyquist plots of Si-C-G (red curve) and Si-C-N-G (blue curve) in Li-Si half-cell configuration before cycling (a) and after 5 cycles (b).

**SEM image and EDS mapping of Si-C-N-G before cycling**

Figure S7 shows the SEM image (a) and EDS mapping of elements Si (b), F (c), C (d), and O (e) of Si-C-N-G electrode before cycling. The F element is from Nafion coating on the Si particle. The uniform

distribution of F element confirms the uniform coating of Nafion on Si particles.

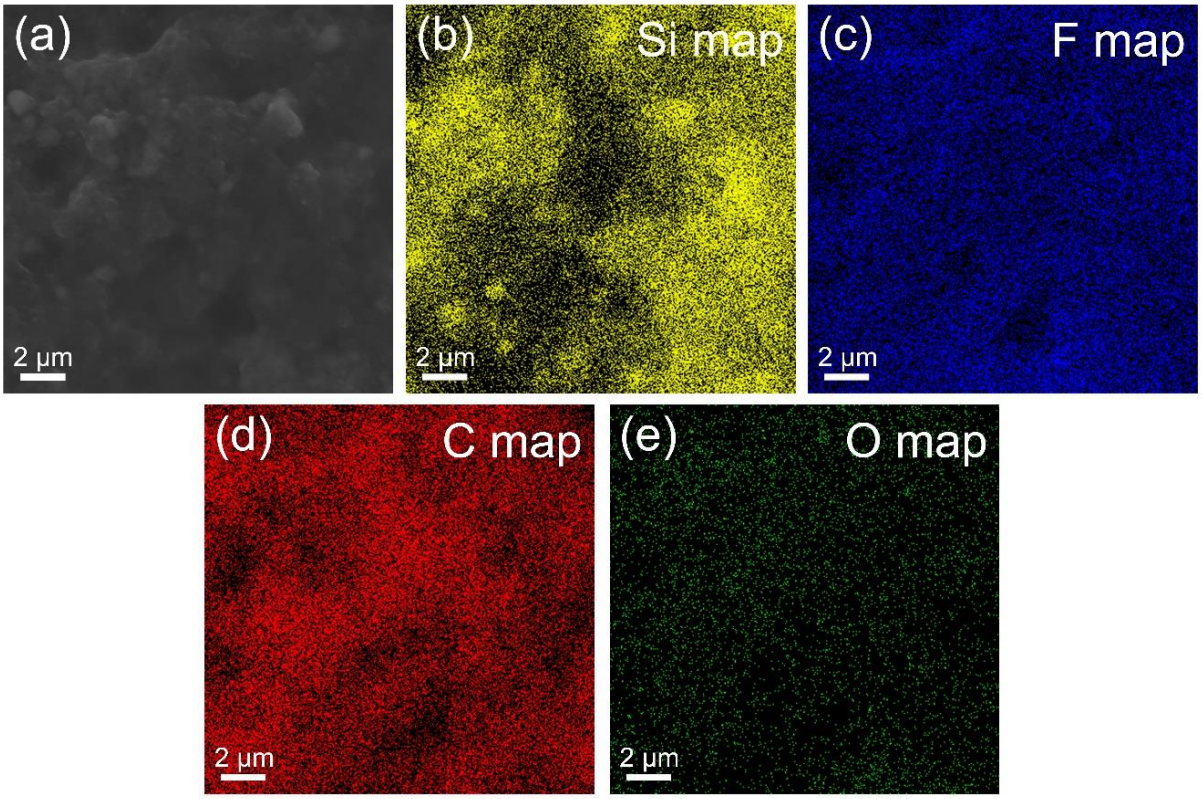


**Figure S7** SEM image (a) and EDS mapping of the elements Si (b), F (c), C (d), and O (e) of Si-C-N-G before cycling.

**SEM image and EDS mapping of Si-C-N-G after cycling in full-cell configuration for 100 cycles.**

Figure S8 shows the SEM image (a) and EDS mapping of elements Si (b), S (c), F (d), C (e), and O (f) of Si-C-N-G electrode after cycling in full-cell configuration for 100 cycles. The Si-C-N-G electrode was disassembled at delithiated state and dried in Ar-protected environment for 12 hours before characterization. It is challenging to observe detailed microstructure of the particles because the electrode contains a mixture of Si-C-N-G, electrolyte, binder, carbon black, and SEI on the surface of particles [13]. The S and F elements distribute uniformly across the electrode, which may demonstrate the uniform Nafion coating after cycling.

However, as the electrolyte contains both S and F elements and SEI may also contain these two elements, we can not conclude that these two elements are solely from Nafion.

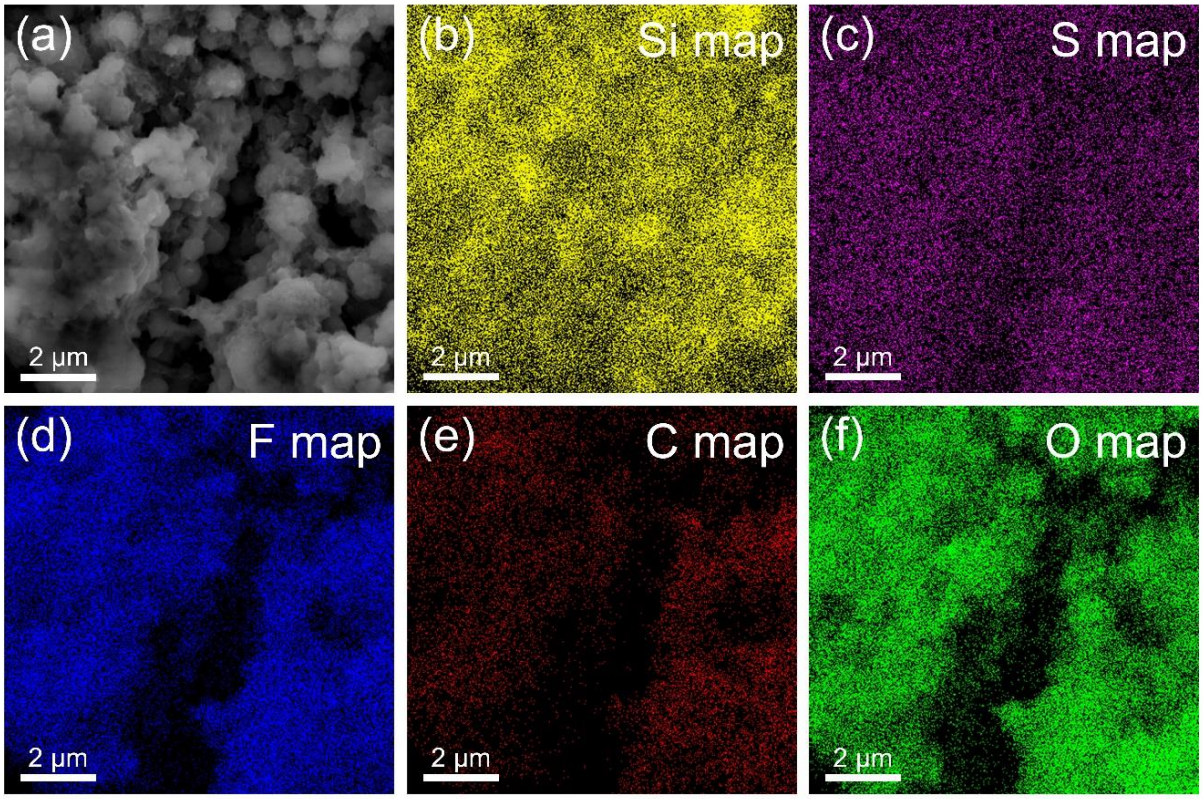


**Figure S8** SEM image (a) and EDS mapping of the elements Si (b), S (c), F (d), C (e), and O (f) of Si-C-N-G after cycling in full-cell configuration for 100 cycles.

## References

[1] Y. Diao, K. Xie, S. Xiong, X. Hong, J. Electrochem. Soc. 159 (2012) A1816-A1821.

[2] D. E. Arreaga-Salas, A. K. Sra, K. Roodenko, Y. J. Chabal, C. L. Hinkle, J. Phys. Chem. C 116 (2012) 9072-9077.

[3] R. Demir-Cakan, M. Morcrette, Gangulibabu, A. Gueguen, R. Dedryvere, J. M. Tarascon, Energy Environ. Sci. 6 (2013) 176-182.

[4] D. Aurbach, E. Pollak, R. Elazari, G. Salitra, C. S. Kelley, J. Affinito, J. Electrochem. Soc. 156 (2009) A694-A702.

[5] A. V. Naumkin , A. Kraut-Vass , S. W. Gaarenstroom , C. J. Powell , NIST Standard Reference Database 20, Version 4.1, http://srdata.nist.gov/xps/.

[6] E. A. Dalchiele, A. Aurora, G. Bernardini, F. Cattaruzza, A. Flamini, P. Pallavicini, R. Zanoni, F. Decker, J. Electroanal. Chem. 579 (2005) 133-142.
[7] E. Radvanyi, E. De Vito, W. Porcher, S. J. S. Larbi, J. Anal. At. Spectrom. 29 (2014) 1120-1131.
[8] F. Xia, S. Kwon, W. W. Lee, Z. Liu, S. Kim, T. Song, K. J. Choi, U. Paik, W. Il Park, Nano Lett. 15 (2015) 6658-6664.
[9] E. Barsoukov, J. H. Kim, J. H. Kim, C. O. Yoon, H. Lee, J. Electrochem. Soc. 145 (1998) 2711-2717.
[10] J. Guo, A. Sun, X. Chen, C. Wang, A. Manivannan, Electrochim. Acta 56 (2011) 3981-3987.
[11] Z. Ogumi, T. Abe, T. Fukutsuka, S. Yamate, Y. Iriyama, J. Power Sources 127 (2004) 72-75.
[12] M. Gaberscek, J. Moskon, B. Erjavec, R. Dominko, J. Jamnik, Electrochem. Solid State Lett. 11 (2008) A170-A174.
[13] Y. Cao, X. Li, I. Aksay, J. Lemmon, Z. Nie, Z. Yang, J. Liu, Phys. Chem. Chem. Phys. 13 (2011) 7660-7665.